Estimating the water budget components of irrigated crops: Combining the FAO-56 dual crop coefficient with surface temperature and vegetation index data

Luis Enrique Olivera-Guerra, Olivier Merlin, Salah Er-Raki, Said Khabba, Maria-José Escorihuela

Estimating the water budget components of irrigated crops: combining the FAO-56 dual crop coefficient with surface temperature and vegetation index data

Luis Olivera-Guerra[1*], Olivier Merlin[1,3], Salah Er-Raki[2], Saïd Khabba[3], Maria Jose Escorihuela[4]

** mail (olivera-guerrale@cesbio.cnes.fr)*

[1] Centre d'Etudes Spatiales de la Biosphère (CESBIO), Université de Toulouse, CNES, CNRS, IRD, UPS, Toulouse, France

[2] LP2M2E, Département de Physique Appliquée, Faculté des Sciences et Techniques, Université Cadi Ayyad, Marrakech, Morocco

[3] LMME, Faculté des Sciences Semlalia, Université Cadi Ayyad, Marrakech, Morocco

[4] isardSAT, Marie Curie 8-14, Parc Tecnològic Barcelona Activa, Barcelona, Catalunya

ABSTRACT

The FAO-56 dual crop coefficient (FAO-2Kc) model has been extensively used at the field scale to estimate the crop water requirements by means of the simulated evapotranspiration (ET) and its two components evaporation (E) and transpiration (T). Given that the main limitation of FAO-2Kc for operational irrigation management over large areas is the unavailability (over most irrigated areas) of irrigation data, this study investigates the feasibility 1) to constrain the FAO-2Kc ET from LST and VI data, 2) to retrieve irrigation amounts and dates from LST and VI data and 3) to estimate the root-zone soil moisture (RZSM) at the daily scale. In practice, the vegetation and soil temperatures retrieved from LST/VI data are used to estimate the FAO-2Kc vegetation stress coefficient (Ks) and soil evaporation reduction coefficient (Kr), respectively. The modeling and remote sensing combined approach is tested over a wheat crop field in central Morocco, and results are evaluated in terms of ET, irrigation and RZSM estimates.

ET is estimated with a RMSE of 0.68 mm day^{-1} compared to 0.84 mm day^{-1} for the standard (without using LST data) FAO-2Kc based on tabulated values for the parameters. The total irrigation depth (67 mm) is correctly estimated and is very close to the actual effective irrigation (69.8 mm) applied by the farmer. Daily RZSM is estimated with an R^2 value of 0.68 (0.42) and a RMSE value of 0.034 (0.061) m^3 m^{-3} by forcing FAO-2Kc using the retrieved irrigation (from LST-derived estimates and precipitation only). Since spaceborne LST data are currently not available at both high-spatial and high-temporal resolution, a sensitivity analysis is finally undertaken to assess the potential and applicability of the proposed methodology to temporally-sparse thermal data.

Keywords: Evapotranspiration, Root-Zone Soil Moisture, Irrigation, FAO-56, Surface Temperature.

1. Introduction

Agriculture is an important pressure on water resources, especially in arid and semi-arid regions where irrigation can consume more than 80% of the available water (Chehbouni et al., 2008; Jarlan et al., 2015). Accurate estimation of evapotranspiration (ET), which critically depends upon the root-zone soil moisture (RZSM), is hence paramount to determine the crop water requirements and consequently to optimize the on-farm irrigation management.

The FAO-56 dual crop coefficient (FAO-2Kc, Allen et al., 1998) model has been extensively used at the field scale to estimate the crop water requirements by means of the simulated ET. In FAO-2Kc, the total ET is partitioned between the soil evaporation (E) and the plant transpiration (T) by using a daily water balance for the topsoil layer and the root-zone,

respectively. This model is often chosen for its simplicity and operational basis as it requires few input data comprised of phenological, standard meteorological and irrigation data. In addition, FAO-2Kc provides quite acceptable ET estimates when compared to more physically based -but often over-parameterized models (Allen, 2000; Er-Raki et al., 2008; Kite and Droogers, 2000). To better constrain the phenological stages in the FAO model, the basal crop coefficient (Kcb) has been related to satellite based vegetation index (VI) (Er-Raki et al., 2010, 2007; González-Dugo and Mateos, 2008; Hunsaker et al., 2005), showing a significant improvement. However, its operational application to large scales (e.g. irrigation perimeter) still faces two critical issues: 1) the unavailability (over most irrigated areas) of real- or near-real time irrigation data at the field scale, and 2) the difficulty in modeling RZSM from meteorological data alone.

In other hand, land surface temperature (LST) derived in the thermal infrared has been widely used for estimating ET and water stress indices (e.g. Kalma et al., 2008; Li et al., 2009). LST has been also assimilated into the FAO method (Er-Raki et al., 2008), and more recently, used in FAO-2Kc to retrieve the water stress coefficient (Ks) (Dejonge et al., 2015; Ihuoma and Madramootoo, 2017; Kullberg et al., 2016). Among the variety of available approaches, the so-called contextual approach is quite attractive for operational applications, as it requires few input data. Contextual ET models estimate the ratio of actual ET to either potential ET (Moran et al., 1994) or available energy by using the remotely sensed LST – VI (Long and Singh, 2012) and/or LST – albedo space (Merlin, 2013; Roerink et al., 2000). In addition to the demonstrated utility of LST for estimating ET, its use has been extended to the retrieval of other components of the water budget, including RZSM (Calvet et al., 1998; Crow et al., 2008).

The relationship between RZSM and LST is explained by the link of the canopy temperature to the T rate under water-stress conditions, that is when RZSM is not

sufficient to maintain a potential T rate (Boulet et al., 2007; Hain et al., 2009; Moran et al., 1994). Several studies have hence derived RZSM through the assimilation of LST or thermal-based proxy variables into land surface models (Calvet et al., 1998; Crow et al., 2008; Hain et al., 2012; Li et al., 2010). Moreover, with Landsat and ASTER thermal data, the spatial resolution that is potentially achievable for RZSM retrievals is 100 m. Note however that one key step in the estimation of thermal-based RZSM estimates over partially vegetated surfaces is the partitioning of the observed LST into soil and canopy temperatures (Merlin et al., 2014, 2012; Moran et al., 1994). Moran et al. (1994) proposed the water deficit index (WDI) to estimate a most probable range of crop water stress over partially vegetated pixels, which is obtained from the aforementioned LST – VI space (contextual method). This crop water stress index is equivalent to the RZSM normalized by the soil moisture at field capacity and by the soil moisture at wilting point (Bastiaanssen et al., 2000). In the FAO formalism, the same thresholds are set for Ks equal to 1 (soil moisture at field capacity) and for a Ks equal to 0 (soil moisture at wilting point). In order to take advantage of: i) the simplicity and robustness of the thermal-based contextual ET models, ii) the utility of LST/VI data for water budget components (E/T, RZSM) and iii) the availability of LST/VI data at a spatial resolution suitable for monitoring crops; this study proposes an original approach to better constrain the water budget components of FAO-2Kc from LST and VI data. In practice, the approach seeks to retrieve the irrigation volumes and dates from first-guess (LST-derived) ET and RZSM, and to re-analyze all water-budget components (including ET and RZSM) from the retrieved irrigation data. In this study, the new methodology is tested by using ground-based observations of LST/VI, evaluated against ET, RZSM and irrigation observations. A sensitivity analysis is carried out in order to assess the applicability of the approach to remote sensing data.

2. Data sets

The experimental site (31°40'9.46"N, 7°35'45.64"O, 575 m above mean sea level) is located over an irrigated area in the semi-arid Haouz plain in the centre of Morocco (Fig. 1). The study focuses on a winter wheat crop, which is an irrigated unit that includes six fields of 4 ha each, from January to May 2003. More details about the experimental site can be found in Duchemin et al. (2008, 2006), Er-Raki et al. (2007) and Toumi et al. (2016). Variables of the surface energy and water balance as well as soil and vegetation characteristics were monitored during the entire growing cycle. The data set is described below.

2.1. Meteorological and flux data

Meteorological data including air temperature, solar radiation, relative humidity and wind speed were monitored throughout the agricultural season at a semi-hourly time step from January 14 until May 27, 2003. The four components of net radiation were measured by using a CNR1 radiometer (Kipp and Zonen). An eddy covariance (EC) system was installed over a winter wheat field to measure the latent and sensible heat fluxes. The data were recorded from high frequency (10 Hz) measurements of turbulent structures: a 3D sonic anemometer (CSAT3, Campbell Scientific), which measured the fluctuations in the wind velocity components and temperature; and an open-path infrared gas analyzer (Li7500, Licor), which measured concentration of water vapor and carbon dioxide.

2.2. Soil moisture data

Six time domain reflectometry (TDR) probes (CS615, Campbell Scientific) were installed in a soil pit near the fluxes measurement tower to measure soil water content at different

depths (5, 10, 20, 30, 50 and 100 cm) every 30 min. The average ground-based RZSM ($RZSM_{obs}$) was estimated by interpolating the soil moisture observations of the different depths belonging to the root-zone of wheat as follows:

$$RZSM_{obs} = \frac{d_i SM_{d_i} + (d_{i+1} - d_i) SM_{d_{i+1}} + \cdots + (d_n - d_{n-1}) SM_{d_n}}{d_i + (d_{i+1} - d_i) + \cdots + (d_n - d_{n-1})} \quad (1)$$

where SM_{di} (m^3m^{-3}) is the soil moisture measured at depth d_i (5 – 100 cm) and d_n is the deeper depth where there is a measurement that belongs to the root-zone. In this study, it is assumed that rooting depth varies according to the crop growth stages, so that different measurements are considered in the Eq. (1). The variation and values of rooting depth is detailed in the section 3.1.2.

2.3. Irrigation data

Four irrigation events were applied in the field along the growing season by flooding with about 24 mm of water regardless of the precipitation and thus of soil moisture conditions. The sowing and the irrigation dates are listed in Table 1.

2.4. Fractional green and total vegetation cover

Given that green vegetation cover is commonly estimated from remote sensing data using empirical relations with vegetation indices, in this study the fractional green vegetation cover (fvg) is estimated from a linear relationship with NDVI (Normalized Difference Vegetation Index) as in Gutman and Ignatov, 1998:

$$f_{vg} = \frac{NDVI - NDVI_s}{NDVI_v - NDVI_s} \quad (2)$$

where NDVI is the near-infrared to red reflectance difference divided by their sum and $NDVI_s$ and $NDVI_v$ correspond to NDVI for bare soil (fvg = 0) and fully covering green vegetation (fvg = 1), respectively. The $NDVI_s$ was equal to the minimum value measured in the field (0.14) and $NDVI_v$ was defined at 0.93 after looking at maximum values taken on individual plots over the study area (Duchemin et al., 2006). Ground-based surface reflectance data over the field were collected using a MSR87 multispectral radiometer (Cropscan Inc., USA) every week. Fifteen sets of canopy reflectance measurements were made between January 8 and May 27 2003. More details about the NDVI measurement procedure can be found in Er-Raki et al. (2007). The fractional total vegetation cover (fc) is derived from fvg by assuming that once fvg has reached its maximum value, it keeps equal to this maximum value until the end of the study period. fc was also measured using a hemispherical digital camera equipped with a fisheye lens with a field-of-view of 183°. Comparing the fvg- and photo-derived fc estimates before the maximum value of fvg revealed a good agreement (data not shown here). The values of root mean square error (RMSE) and coefficient of determination (R^2) were equal to 3.5% and 1.0, respectively.

2.5. Land Surface Temperature

In situ LST was derived from tower-based measurements of thermal radiances emitted from the surface, which were sampled at 1 Hz and averaged over 30 min. The averaged radiance was converted to LST by inverting Planck's law:

$$B(LST) = \frac{Lrad - (1-\varepsilon)Ldown}{\varepsilon} \quad (3)$$

where *Lrad* is the land leaving radiance (W m^{-2}) measured by a thermal radiometer (SI-111, Apogee), ε is the land surface emissivity, *Ldown* is the long-wave downwelling irradiance (W m^{-2}) and *B(LST)* is Planck's law for the *LST* (W $m^{-2}sr^{-1}\mu m^{-1}$). *Ldown* was retrieved from the incoming longwave radiation measurement from the net radiometer (CNR1, Kipp & Zonen). The ε was retrieved from the simplified NDVI threshold method (Sobrino et al., 2008) that weights the soil and vegetation emissivity through the fractional green vegetation cover (fvg). The soil emissivity was measured by Olioso et al. (2007) over the study area and the vegetation emissivity was considered equal to 0.99 (Amazirh et al., 2017, Sobrino et al., 2008). Only the 30-min LST data collected between 10 am and 2 pm are used in this study, consistent with the overpass times of current thermal satellite missions (e.g. ASTER, Landsat, MODIS). In addition to the radiometric LST, the vegetation temperature was measured with Type-J thermocouples (seven replications, one sensor per plant), which were clumped on the vegetation apex near the location of the thermal radiometer. The sensors were changed every week to be set up at the vegetation apex and to measure the youngest leaves of the plant along the growing season. Thermocouple measurements will be used to evaluate the vegetation temperature estimates from the partition method of LST.

3. Methodology

3.1. Overview of FAO-56 dual crop coefficient method

The FAO-2Kc is a water balance model driven by 1) meteorological forcing variables to calculate reference evapotranspiration ET_0 and 2) precipitation and irrigation that jointly

determine the water supply to simulate the soil water availability for soil evaporation and plant transpiration. In practice, FAO-2Kc estimates ET by multiplying ET_0 by a two separate crop coefficients:

$$ET = (KsKcb + Ke)ET_0 \quad (4)$$

where Kcb is the basal crop transpiration, Ks the stress coefficient (0-1) that represents the vegetation water status and a reduction factor of T (Kcb ET_0) and Ke the evaporation coefficient. ET_0 is calculated according to the FAO Penman–Monteith equation (Allen et al., 1998) at daily scale. The values used for Kcb (Kcb_{ini}, Kcb_{mid} and Kcb_{end}) at the three crop growth stages (initial, mid-season and maturity respectively) were taken from Allen et al. (1998). Ks (unitless) is calculated based on daily computation of the water balance for the root-zone layer Zr (m) as follows:

$$K_s = \frac{TAW - D_r}{TAW - RAW} = \frac{TAW - D_r}{TAW(1 - p)} \quad (5)$$

where Dr (mm) is root zone depletion, TAW (mm) is total available soil water in the root zone, and p is the fraction of TAW that a crop can extract from the root zone without suffering from water stress. Water stress occurs when Dr becomes greater than RAW (Ks < 1). In contrast, when Dr ≤ RAW, Ks = 1 (see Fig. 3). Dr is calculated from the daily water balance. TAW is estimated as the difference between the water content at field capacity (SM_{FC}) and wilting point (SM_{WP}) by the daily crop rooting depth (TAW = 1000 (SM_{FC} – SM_{WP}) Zr). The rooting depth Zr is assumed to vary between a minimum value (maintained during the initial crop growth stage at 0.1 m) and a maximum value (reached

at the beginning of the mid-season stage). The maximum value was measured in the field and was equal to 0.52 m according to Er-Raki et al. (2007). The soil parameters SM_{FC} and SM_{WP} were considered equal to an average value of 0.37 and 0.17 m^3m^{-3} respectively, in accordance with the values recommended by Allen et al. (1998) and with the minimum and maximum SM observed in the root-zone for the agricultural season.

3.2. LST-integrated FAO-2Kc: new approach in the calculation of water budget components

Given that the main limitation of FAO-2Kc for operational irrigation management over large areas is the unavailability (over most irrigated areas) of irrigation data at the field scale, a new approach (named LST-integrated FAO-2Kc) is proposed to derive the water budget components from LST and VI data. An overview of the methodology is represented in Fig. 2 and is explained below.

Basically, LST is integrated in the standard FAO-2Kc at two levels: the ET and SM modeling components. LST is first partitioned into its soil and vegetation components to force E and T separately via thermal-derived estimates of Ks and Kr, respectively (ET modeling component). Note that the thermal-derived Ks is also used to derive a first-guess (LST-derived) RZSM estimate, based on the FAO-2Kc relationship between TAW and Ks (SM modeling component). The dynamic of first-guess RZSM is then analyzed to retrieve the irrigation amounts and dates. The FAO-2Kc is next forced by the previously retrieved irrigation and re-analyzed estimates of RZSM ($RZSM_{FAO+LST}$) and ET ($ET_{FAO+LST}$) are finally provided. The different components of LST-integrated FAO-2Kc (namely LST partitioning, thermal-derived Ks and Kr, first-guess ET and RZSM, irrigation retrieval, and re-analyzed ET and RZSM) are described in the following sections.

3.2.1. Partitioning LST

The method used for partitioning LST into vegetation and soil components relies on the combination between the hourglass approach (Moran et al., 1994) and the procedure to obtain the Temperature Vegetation Dryness Index (Sandholt et al., 2002). These two methods are based on the polygon defined in the LST – VI space. Ts_{max} is the temperature of a fully dry bare soil. Ts_{min} is the temperature of a fully wet bare soil. Tv_{max} is the maximum vegetation temperature corresponding to fully stressed (non-transpiring) vegetation. Tv_{min} is the minimum vegetation temperature corresponding to well-watered unstressed vegetation (transpiring at potential rate). Since this study tests the feasibility of the proposed methodology from in situ measurements, the image-based polygon cannot be plotted to constrain the temperature endmembers (Ts_{max}, Ts_{min}, Tv_{max}, Tv_{min}). Therefore, these temperatures are simulated by using the energy balance model proposed by Stefan et al. (2015). Ts_{min} and Ts_{max} are simulated by a soil energy balance model, while Tv_{min} is set to the air temperature and Tv_{max} is defined according to the assumptions that the difference between Ts_{max} and Ts_{min} is the same that between Tv_{max} and Tv_{min} (Stefan et al. 2015). Once the temperature endmembers have been defined, Tv is obtained by using the hourglass approach or TVDI method according to the position of the (fc, LST) point in the polygon. In practice, the diagonals are plotted in the polygon LST – fc space by distinguishing four areas (evaporation- and transpiration-controlled, unstressed and stressed mixed surface), as they were defined in Merlin et al. (2012). If the (fc, LST) point belongs to the unstressed mixed or stressed mixed zone, Tv is calculated according to Merlin et al. (2012). If the (fc, LST) point belongs to the evaporation-controlled or transpiration-controlled zone, Tv is calculated by using the TVDI method, by interpolating the temperature between the Tv_{max} and Tv_{min}.

Derivation of Ts is based on a linear decomposition of the LST into its soil and vegetation components as a good approximation of the relationship with fourth power for temperatures (and consistent with the contextual approach) as follows:

$$Ts = \frac{LST - fcTv}{1 - fc} \tag{6}$$

3.2.2. Retrieving stress coefficient (Ks) and evaporation reduction coefficient (Kr) from thermal data

LST data are used to reflect the soil and crop water status by calculating stress indices for the surface and root-zone layer, respectively, namely the E reduction coefficient (Kr), and the stress coefficient (Ks). The Ks (Kr) was estimated by relating the vegetation (soil) temperature to cold and hot extreme temperatures of vegetation (soil) that represent wet and dry vegetation (soil) as follows:

$$Kr_{LST} = \frac{Ts_{max} - Ts}{Ts_{max} - Ts_{min}} \tag{7}$$

$$Ks_{LST} = \frac{Tv_{max} - Tv}{Tv_{max} - Tv_{min}} \tag{8}$$

where Ts and Tv correspond to the temperature of the soil and vegetation component derived from the partitioning method presented above.

Given that we have daily LST observation, Ks_{LST} may show significant day-to-day variability associated with uncertainties in the LST partitioning method, the LST-derived

Ks was smoothed to reduce random uncertainties. A weighting function is applied to the Ks_{LST} values estimated during a 3-day sliding period:

$$Ks_{LST,cor,i} = \sum_{i-1}^{i+1} \frac{w_i Ks_{LST,i}}{\sum w_i} \quad ; \quad w_i = 1 - \frac{error}{Tv_{max,i} - Tv_{min,i}} \tag{9}$$

where $Ks_{LST,cor,i}$ is the smoothed Ks_{LST}, w_i (0 – 1) is the weight corresponding to the Ks_{LST} of day i and the subscript '*i–1*' and '*i+1*' is referred to the day before and after, respectively. The *error* is the uncertainty considered for the LST partitioning method (i.e. uncertainty in Tv estimates). We define the weight w_i such as: i) the higher the (Tv_{max} – Tv_{min}) difference, the higher the weight w_i, and ii) w_i is set to 0 for (Tv_{max} – Tv_{min}) < *error*. The smoothing procedure become necessary since RZSM is derived from thermal-derived Ks and to obtain a temporal dynamic more consistent with RZSM observations.

3.2.3. First-guess ET

A thermal-based ET (ET_{LST}) is calculated by using the FAO-2Kc formulation (Eq. (4)) and the coefficients Kr_{LST} and Ks_{LST} (Eq. (7) and (9)).

3.2.4. First guess RZSM

The procedure to estimate first-guess (LST-derived) RZSM is described below. RZSM can be derived from the root-zone depletion (D_r) and the soil parameter used in the FAO-56 formalism (SM_{WP}, SM_{FC}, TAW) as follows:

$$RZSM = SM_{WP} + \left(1 - \frac{D_r}{TAW}\right)(SM_{FC} - SM_{WP}) \tag{10}$$

By inserting the Eq. (5) into the Eq. (10), RZSM is expressed as a function of Ks during stressed periods (Ks<1, Dr<RAW):

$$RZSM = SM_{WP} + Ks_{LST}(1-p)(SM_{FC} - SM_{WP}) \quad (11)$$

Note that for unstressed periods (Ks = 1), RZSM from Eq. (11) would be equal to the threshold from which the stressed conditions end ($SM_{Threshold}$). According to the values of SM_{WP}, SM_{FC} and p used in this study (0.17, 0.37 and 0.55, respectively), the $SM_{Threshold}$ is equal to 0.26. During unstressed periods, RZSM from Eq. (11) is thus corrected dynamically for both cumulated precipitation and cumulated ET_{LST} during this period through a daily water balance (shaded area in plot of Fig. 3). The RZSM is limited to a maximum of SM_{FC}. If this maximum is reached then the RZSM is reset to the $SM_{Threshold}$ and next the above correction is applied. For instance, in the Fig. 3, $RZSM_{LST,cor}$ would reach SM_{FC} if the unstressed period were longer and then it would be reset to the $SM_{Threshold}$ to carry on the correction in the unstressed period remaining.

3.2.5. Irrigation retrieval

Irrigation events are detected based on a significant increase in first-guess (LST-derived) RZSM, which cannot be attributed to precipitation. Only significant increases are considered with a RZSM change larger than a threshold value equal to 0.02 m^3m^{-3}, which represents a water supply greater than 10 mm for a 0.5 m root-zone depth. Note that such a threshold considers that ET and drainage are both negligible compared to the irrigation depth (during the irrigation event), and that the irrigation depth is larger than 10 mm. For the periods with steady increase in RZSM, the amount of retrieved/inverted irrigation (I_{inv}) is constrained through a water budget between the amounts of precipitation as

inflow and the LST-derived ET as outflow, as well as the drainage if it is produced by precipitation.

The periods when a significant man-made water supply is observed are considered as probable dates for the retrieved irrigation events. If an irrigation is effectively detected for this period (with a minimum threshold of 10 mm), then the estimated date of irrigation is set as the last date of the period, in order to agree the maximum LST-based RZSM and the maximum RZSM simulated from FAO-56.

3.2.6. Re-analyzed RZSM and ET

Once irrigation has been retrieved from first-guess (LST-derived) RZSM, first-guess ET and observed precipitations, the standard FAO-2Kc is implemented by using the default (non-calibrated) parameters given by Allen et al. (1998), but with the difference that the retrieved irrigation (amounts and dates) is introduced as forcing. From the FAO-2Kc we obtained ET, E, T as well as Dr and TAW that allow us to calculate RZSM by using the Eq. (10) throughout the growing season. Note that Eq. (10) is valid to obtain the RZSM for both stressed and non-stresses periods, because Dr is calculated from the daily water balance implemented in FAO-2Kc for its full range ($0 \leq Dr \leq TAW$). To distinguish the simulated ET and RZSM from their first-guess (LST-derived) values, the former are referred to as re-analyzed RZSM and ET, respectively.

3.3. Validation strategy of irrigation, ET and RZSM estimates

In this study, the validation is carried out in terms of ET, RZSM and irrigation estimates by comparing them against ground-based ET, RZSM and actual irrigation on a daily basis. Two evaluations are performed for ET and RZSM estimates: 1) LST-derived (or first-

guess) estimates and 2) derived from standard FAO-2Kc forced by retrieved irrigation. The irrigation is assessed in terms of dates and amounts. Regarding dates, the irrigation is compared in terms of 1) the numbers of retrieved irrigation events and 2) the agreement between probable dates on which the irrigation is detected and the actual date of the events. Regarding amounts, two scales are considered for the cumulated irrigation: the daily and seasonal time scales. However, taking into account that irrigation is estimated by assuming a negligible drainage (during irrigation periods), the retrieved irrigation is compared to the observed irrigation after subtracting the drainage. Since no measurement was available during the field experiment, drainage was estimated from the standard FAO-2Kc using observed irrigation as forcing.

4. Results

4.1. LST partitioning

In Fig. 4 is shown the series of soil (Ts, Ts_{min} and Ts_{max}) and vegetation (Tv, Tv_{min} and Tv_{max}) temperatures. According to the partition method, Ts and Tv are estimated within its corresponding endmembers and the ground-based LST (LST_{obs} in Fig. 4) is observed within the minimum and maximum temperatures (Tv_{min} and Ts_{max}, respectively) for practically the whole season. Thus temperature endmembers are suitably simulated, fully consistent with LST observations.

In order to validate quantitatively the partition of LST into its vegetation (Tv) and soil (Ts) components, Tv is compared against the mean vegetation temperature from the seven thermocouples set up in the vegetation apex. The RMSE and R^2 are equal to 3.27 °C and 0.92, respectively. Note that if the validation daytime period is restricted between 10 am and 1 pm only (still consistent with the overpass time of thermal missions such as ASTER, Landsat and MODIS), the errors are improved reaching a RMSE of 2.98 °C. These results

are similar to the errors obtained by Stefan et al. (2015) for the simulation of the soil temperature endmembers (Ts_{max}, Ts_{min}) over the same study area. It can be observed in Fig. 5 that Tv is overestimated for values larger than 30 °C, corresponding to the late season (after DAS 120). This is due to location (in the apex) of the Tv measurements. Indeed, the youngest leaves of the plant are expected to be colder (with a higher transpiration rate) than the adult and senescing leaves, whose temperature has not been measured. Another reason can be probably explained for the impact of water stress on surface roughness (vegetation height), which was neglected in the estimation of Tv_{max} and Tv_{min}. The four temperature endmembers and the decomposed temperatures (Tv, Ts) are then used in Eqs. (8 – 10) to estimate the E and T reduction factors (Kr_{LST} and Ks_{LST}, respectively).

4.2. LST-derived ET estimates

Two versions of the FAO-2Kc method are compared: the standard version by using the parameters given in Allen et al. (1998) forced by the observed irrigation, and the version proposed in this study by using the Kr_{LST} (Eq. (7)) and Ks_{LST} (Eq. (8)) coefficients derived from LST/VI data. Comparison between the time series of vegetation stress coefficient from standard FAO-2Kc (Ks_{FAO}) and from LST/VI (Ks_{LST}) is presented in Fig. 6. Overall, Ks_{LST} detects stress periods and responds well to the water inputs (see the significant increase just after irrigation events), even though its estimation is fully independent of the daily water balance. However, it shows day-to-day variability that could be associated with uncertainties in the LST partitioning method (errors in Tv estimates). For this reason, the LST-derived Ks is smoothed to reduce random uncertainties, by using the Ks_{LST} values estimated on the day before and the day after (Eq. (9)). It can be observed that LST-derived Ks simulates stress conditions in a more pronounced way than the

standard FAO-2Kc, except for the late season. Such information can next be used to simulate the required water supply (see section 4.3).

The evolution of ET during the growing season is simulated by both FAO-2Kc versions (Fig. 7). Results show that the performance of the FAO-2Kc by using coefficients based on LST/VI is superior to that of the standard version. The ET is estimated with an RMSE equal to 0.84 and 0.68 mm.day^{-1} by using the standard FAO-2Kc and the proposed method, respectively. The main discrepancies between both methods can be observed during the development (between DAS 40 and 70) and late (after DAS 110) stages due to great differences in Ks estimates and thus in T. Late in the season (after DAS 110) a difference in E estimates is also observed, according to daily water balance used in FAO-2Kc the water in surface evaporable layer is fully depleted (Kr_{FAO} = 0, E = 0), whereas the LST-derived E increases to about 1 mm day^{-1} because Ts is estimated between Ts_{max} and Ts_{min} from the partition of LST and thus Kr_{LST} is larger than 0. The increase in E can be explained by an increase of i) the sun-exposed soil due to the reduction of vegetation and ii) the capillary rise from the root zone, which can be detected from the LST-derived E estimates although the fc was assumed constant after the fc peak. A recent study about the E/T partitioning of winter wheat (Rafi et al., 2018) noted an underestimation of E by FAO-56 especially during the senescence period, consistent with the thermal-derived E estimates of this study. In the same way, others differences in E is found in the initial stage (before DAS 20) that could not be evaluated due to the lack of in situ measurements. Discrepancies are also observed when comparing each method individually against the observed ET. During the first period (DAS 40 – 70), ET is overestimated with the standard FAO-2Kc while it is underestimated with FAO-2Kc constrained by LST/VI data, whereas the opposite situation is encountered during late season, although the errors for the modified FAO-2Kc are lower.

Note that the ET and T estimated by using the LST-derived Ks or the smoothed LST-derived one are almost the same (Fig 7b). Also, the RMSE and slope for ET are slightly improved by using the smoothed LST-derived Ks from 0.70 to 0.68 mm day^{-1} and from 1.10 to 1.07, respectively. Nonetheless, it is worth noting that the smoothing is more useful in the estimation of RZSM from Eq. (11) by reducing the noisy temporal variability from thermal data (Ks_{LST}) and by obtaining a temporal variability more consistent with the temporal dynamic of the observed RZSM.

4.3. Irrigation estimates

The calculation of RZSM from Ks_{LST} (Eq. 11) and its variations allowed the detection of the irrigation time. In Fig. 8 it can be observed that four probable irrigation events were identified, corresponding to significant increases in LST-derived RZSM. Note that the probable days for an irrigation supply are marked in cyan in Fig. 8. Every identified event is in good agreement with the observed irrigation. However, only three irrigation events were detected from the inversion of the water budget whereas four probable events were obtained from significant increases in $RZSM_{LST}$. The probable event detected on DAS 86 – 90 does not correspond to a retrieved irrigation event. This is due to the rainfall events on DAS 86 – 87, which resulted in relatively high RZSM values, so that the LST-derived RZSM was not sensitive enough to an additional (man-made) water supply on DAS 91. Given that the last two actual irrigation events were applied 8 days apart and because three rainfalls occurred between both events, it was difficult to differentiate both irrigation supplies. This may be the reason for the overestimation of the irrigation amount of the last event (irrigation is estimated as 39.6 mm compared to 24 mm for the assumed true value).

The total irrigation depth for the growing season was equal to 67 mm, that represents a relative error of 30.2 % compared to the total irrigation applied by the farmer. Note that the retrieved irrigation amounts are only estimated considering the water required to produce the increase in LST-derived RZSM and thus the drainage from irrigation is not taken into account. The total drainage of the irrigation periods simulated along the season by standard FAO-2Kc with observed irrigation as forcing is equal to 26.2 mm. If we subtract this quantity to the observed total irrigation water supply (24 mm x 4 irrigations = 96 mm) the effective irrigation would be equal to 69.8 mm, which is very close to the cumulated retrieved irrigation estimated as 67.0 mm.

4.4. RZSM estimates

The time series for daily first-guess (LST-derived) RZSM and re-analyzed RZSM (RZSM simulated by the FAO-2Kc forced by retrieved irrigation) are shown in Fig. 8, namely $RZSM_{LST}$ and $RZSM_{FAO+LST}$. Also, the time series of the observed RZSM is shown for comparison. The validation for each RZSM product is presented in Fig. 9. It can be observed in both Fig. 8 and 9 that the first-guess RZSM is systematically underestimated with an averaged bias equal to -0.044 m^3m^{-3}. Although the first-guess RZSM shows a poor accuracy with a RMSE of 0.061 m^3m^{-3}, it is shown an acceptable representativeness of the temporal variability of RZSM that can be seen in the ability to detect the irrigation dates and amounts, just as in previous section, and an acceptable R^2 equal to 0.42. $RZSM_{FAO+LST}$ is significantly improved (RMSE of 0.034 m^3m^{-3} and R^2 of 0.68) and the results are very close if the actual irrigation is used as forcing in the FAO-2Kc (RMSE equal to 0.032 m^3m^{-3} and R^2 equal to 0.73). Overall, standard FAO-2Kc is able to estimate the RZSM ($RZSM_{FAO+LST}$) through the Eq. (10), except during rainfall periods (without irrigation) when an overestimation can be observed (Fig. 8 and 9). Hence, the standard FAO-2Kc does

not represent sufficiently well the response of RZSM to the precipitation. This could be an effect of the rain gauges, which generally provide a larger measurement than the effective precipitation due to canopy interception. It can also be assumed that the FAO-2Kc model responds differently to natural and man-made water supplies due to differences in water supply intensities.

Regarding the overestimation during the late season of first-guess RZSM from Eq. (11), and given the overestimation during the same period of LST-derived ET, which are both dependent on LST-derived Ks, we can affirm that the LST-derived Ks during this period is overestimated. This may be due to an overestimation of Tv_{max} (see Fig. 5) during this period with full-cover senescent vegetation. In fact, it is suspected that the assumption $Tv_{max} - Tv_{min} = Ts_{max} - Ts_{min}$ does not apply during senescence period.

5. Discussion

5.1. Utility of thermal data to help constrain the water budget and retrieving root zone soil moisture

Given the results of Ks_{LST} estimates in Fig. 6 it can be observed that Ks_{LST} responds well to water inputs and its dynamic is fully consistent with the water balance estimates (Ks_{FAO}). Moreover, the ET estimated from LST-derived coefficients (ET_{LST}) is more accurate in Fig. 7 than that of the standard FAO-2Kc (ET_{FAO}). The good performance of ET_{LST} can be explained by 1) the strong relationship between the LST and the coupled energy-water balance as recently reported in Diarra et al., (2017) when the TSEB model was used over the wheat field in the same area, 2) and the robustness of contextual models, which do not require accurate LST estimates to obtain satisfying results in ET retrievals (Kalma et al., 2008). In contrast with contextual methods, the standard FAO-2Kc requires local calibration to accurately estimate ET. This was notably demonstrated by Er-Raki et al.

(2007) with the same wheat field. For instance, they found a significant difference between the locally calibrated and non-calibrated Kcb and then ET estimates, indicating that wheat was not growing in optimal conditions. Such conditions can be detected by the proposed approach based on LST-derived coefficients (Ks_{LST} and Kr_{LST}), thus avoiding both the use of parameters (e.g. SM_{FC}, SM_{WP}, Ze, Zr) and the local calibration of Kcb. However, if locally derived Kcb by Er-Raki et al. (2007) is used in the standard FAO-2Kc, better estimates of ET are obtained with a RMSE and R^2 equal to 0.65 mm day^{-1} and 0.81, respectively. Nonetheless, the use of EC measurements for calibration is a strong limitation for application of the methods to large areas. It should be noted that the performance of ET_{LST} is even better than the re-analyzed ET ($ET_{FAO+LST}$) since it is simulated from FAO-2Kc by using the retrieved irrigation and non-calibrated Kcb. In order to improve these estimates, the Kcb could be 1) forced by NDVI and 2) calibrated from ET_{LST} estimates since $ET_{FAO+LST}$ does not take into account the stress detected from LST-estimates (not only the water stress). In this sense the vegetation conditions can be included in the re-analyzed ET through the Kcb calibrated from LST/VI data accounting the ET_{LST} improvement.

LST-derived RZSM ($RZSM_{LST}$) responds well to stressed periods and water inputs, consistent with the control of RZSM on the vegetation stress detected from canopy temperature (Tv). Even though a significant bias is observed in the validation of $RZSM_{LST}$, its range of variability is enough to detect significant increases, which is the basis of the irrigation retrieval procedure. Finally, FAO-2Kc is implemented by using the retrieved irrigation and a re-analyzed RZSM is retrieved with a noticeable improvement. Such results confirm the utility of LST to help constrain the water budget components, and can be used in an irrigation scheduling program for deciding when and how much to irrigate.

5.2. *Applicability to temporally sparse thermal data*

As mentioned in Section 2, this study was undertaken by using ground-based radiometric LST. Therefore, the uncertainty and temporal sampling of remotely sensed LST are not taken into account. Regarding the uncertainty, many studies have demonstrated that contextual models, such as the LST/VI-based method used herein to partition LST, allow us to avoid accurate estimates of surface variables, since the extreme water conditions (stressed – well-watered) used as boundaries to estimate thermal-based evaporative indices are estimated from the variability captured within thermal imagery (Kalma et al., 2008; Li et al., 2009). With regard to temporal sampling, this issue becomes a key limitation of spaceborne thermal sensors due to the restriction of surface retrievals to sufficiently cloud-free days (Crow et al., 2008). In addition to the thermal data currently available at high spatial (100 m) resolution have a repeat cycle of 16 days only, and up to 8 days by combining Landsat-7 and -8. To assess the impact of the observation frequency on the proposed approach, a sensitivity analysis is carried out by decreasing the LST observation frequency. It should be noted that the smoothing of Ks_{LST} (Eq. (9)) to reduce the day-to-day variability is only applied for a daily revisit of LST observations. For a frequency between 2 and 16 days the Ks_{LST} from Eq. (8) is directly used without smoothing to LST-derived estimates. The assessment is undertaken in terms of RZSM, ET and total irrigation water supply simulated by FAO-2Kc.

Increasing the duration between LST observations, naturally leads to a decreasing the number of thermal-derived ET and RZSM retrievals (from Eq. (4) and (11), respectively) available to constrain the irrigation from FAO-2Kc. However, given that irrigation can be estimated, it allows us to run FAO-2Kc for estimating RZSM and ET every day along the season. Fig. 10 shows the impact of the observation frequency every 2, 4, 8 and 16 days on estimating RZSM. One can observe the decreasing number of LST-derived RZSM

estimates ($RZSM_{LST}$), its errors and the significant improvement after running FAO-2Kc model by using the retrieved irrigation. Such approach allows estimating the RZSM for all days during the growing season ($RZSM_{FAO+LST}$) irrespective of the observation frequency used.

Fig. 11 shows the impact on RZSM and ET estimates of the availability of LST observations according to the time revisit frequency ranging from 1 to 16 days. Although even the errors are gradually increasing, the results demonstrate a relatively good performance and acceptable errors by increasing the revisit period. Fig. 12 shows the impact of the availability of LST observations on the retrieved total irrigation water amount and number of irrigation events. Acceptable errors in the total water supply are observed. The number of simulated irrigation events decreases as the time revisit frequency decreases, falling below 3 events with a revisit longer than 8 days. Overall, it might be noted that up to a 10-day revisit of LST observations, a good agreement is obtained with R^2 higher than 0.5 and 0.6 for RZSM and ET respectively, and a mean absolute error (MAE) of total irrigation water supply lower than 15 mm (corresponding to a relative MAE of 21%). According to these results, it could be considered the use of LST products with time revisit of 8 days such as i) the combination of Landsat-7 and -8 LST on cloud-free days and/or ii) the 1 km resolution MODIS LST product downscaled to 100 m resolution by using the Landsat LST (e.g. Anderson et al., 2012; Cammalleri et al., 2014; Olivera-Guerra et al., 2017; Weng et al., 2014).

The results show clearly the applicability to remote sensing data and the utility to the irrigation scheduling at regional scale. Given that Ks_{LST} and irrigation volumes and dates can be fully obtained from remotely sensed LST/VI data, this methodology could be implemented in an irrigation index to characterize the irrigation distribution, such as the irrigation index priority proposed by Belaqziz et al. (2013). This index takes into account

the Ks and the irrigation volumes and dates and by using remote sensed-derived Ks and irrigation would allow evaluate the irrigation scheduling over broad irrigated agricultural areas poorly monitored.

6. Conclusions

A new approach in the calculation of water budget components and for irrigation scheduling (when and how much to irrigate) is developed by integrating LST data into the FAO-2Kc model. It relies on: 1) the estimation of first-guess (LST-derived) RZSM from Ks_{LST} (Ks_{LST} < 1) during stressed periods and its correction for both cumulated precipitation and cumulated ET during unstressed periods (Ks_{LST} = 1); 2) the estimation of irrigation amounts and dates along the season from (first-guess) LST-derived RZSM and ET estimates; and 3) the use of retrieved irrigations to force FAO-2Kc to simulate RZSM and ET on a daily basis. Statistical results indicate that first-guess (LST-derived) ET (ET_{LST}) is more accurate than the ET simulated by the standard version of FAO-2Kc while the first-guess RZSM is significantly improved when FAO-2Kc is implemented by using retrieved irrigation. Results show that the new methodology combining FAO-2Kc and LST/VI data is able to 1) accurately estimate the crop ET using the default (non-calibrated) parameters given by Allen et al. (1998), 2) to estimate the irrigation amounts and dates and 3) to accurately simulate RZSM.

The impact of temporal sampling in LST observation is assessed by carrying out by decreasing the LST observation frequency from 1 to 16 days. It is demonstrated that the irrigation amounts and dates can be estimated, allowing us to run FAO-2Kc for estimating RZSM and ET along the season on a daily basis. Although errors are gradually increasing with the observation period, results demonstrate a relatively good performance and acceptable errors for an observation frequency of 1 per 8 days so it is recommended to

use LST observations at a temporal resolution finer than 10 days. In order to take advantage of the high temporal resolution of MODIS LST and the high spatial resolution of Landsat LST, downscaling method could be included in the future for monitoring the RZSM at the field and daily scale. However, further research will be required to assess the impact of downscaling uncertainties in the proposed methodology.

Acknowledgements

This study was supported by the French Agence Nationale de la Recherche (MIXMOD-E project, ANR-13-JS06-003-01) and the European Commission Horizon 2020 Programme for Research and Innovation (H2020) in the context of the Marie Sklodowska-Curie Research and Innovation Staff Exchange (RISE) action (REC project, grant agreement no: 645642). The *in situ* data set was provided by the Joint International Laboratory TREMA http://trema.ucam.ac.ma. L. Olivera-Guerra acknowledges the support from CONICYT through the PhD fellowship "BecasChile de Doctorado en el Extranjero".

References

Allen, R.G., 2000. Using the FAO-56 dual crop coefficient method over an irrigated region as part of an evapotranspiration intercomparison study. J. Hydrol. 229, 27–41. https://doi.org/10.1016/S0022-1694(99)00194-8

Allen, R.G., Pereira, L.S., Raes, D., Smith., M., 1998. Crop evapotranspiration - Guidlines for computing crop water requirements. Irrig. Drainage. Pap. 56, Food Agriciculture. Organ. United Nations, Rome, Italy.

Amazirh, A., Er-Raki, S., Chehbouni, A., Rivalland, V., Diarra, A., Khabba, S., Ezzahar, J., Merlin, O., 2017. Modified Penman–Monteith equation for monitoring evapotranspiration of wheat crop: Relationship between the surface resistance and remotely sensed stress index. Biosyst. Eng. 164, 68–84. https://doi.org/10.1016/j.biosystemseng.2017.09.015

Anderson, M.C., Kustas, W.P., Alfieri, J.G., Gao, F., Hain, C., Prueger, J.H., Evett, S., Colaizzi, P., Howell, T., Chávez, J.L., 2012. Mapping daily evapotranspiration at Landsat spatial scales during the BEAREX'08 field campaign. Adv. Water Resour. 50, 162–177. https://doi.org/10.1016/j.advwatres.2012.06.005

Bastiaanssen, W.G.M., Molden, D.J., Makin, I.W., 2000. Remote sensing for irrigated agriculture: examples from research and possible applications. Agric. Water Manag.

46, 137–155. https://doi.org/10.1016/S0378-3774(00)00080-9
Belaqziz, S., Khabba, S., Er-Raki, S., Jarlan, L., Le Page, M., Kharrou, M.H., Adnani, M. El, Chehbouni, A., 2013. A new irrigation priority index based on remote sensing data for assessing the networks irrigation scheduling. Agric. Water Manag. 119, 1–9. https://doi.org/10.1016/j.agwat.2012.12.011
Boulet, G., Chehbouni, A., Gentine, P., Duchemin, B., Ezzahar, J., Hadria, R., 2007. Monitoring water stress using time series of observed to unstressed surface temperature difference. Agric. For. Meteorol. 146, 159–172. https://doi.org/10.1016/j.agrformet.2007.05.012
Calvet, J.-C., Noilhan, J., Bessemoulin, P., 1998. Retrieving the Root-Zone Soil Moisture from Surface Soil Moisture or Temperature Estimates: A Feasibility Study Based on Field Measurements. J. Appl. Meteorol. 37, 371–386. https://doi.org/10.1175/1520-0450(1998)037<0371:RTRZSM>2.0.CO;2
Cammalleri, C., Anderson, M.C., Gao, F., Hain, C.R., Kustas, W.P., 2014. Mapping daily evapotranspiration at field scales over rainfed and irrigated agricultural areas using remote sensing data fusion. Agric. For. Meteorol. 186, 1–11. https://doi.org/10.1016/j.agrformet.2013.11.001
Chehbouni, A., Escadafal, R., Duchemin, B., Boulet, G., Simonneaux, V., Dedieu, G., Mougenot, B., Khabba, S., Kharrou, H., Maisongrande, P., Merlin, O., Chaponnière, A., Ezzahar, J., Er-Raki, S., Hoedjes, J., Hadria, R., Abourida, A., Cheggour, A., Raibi, F., Boudhar, A., Benhadj, I., Hanich, L., Benkaddour, A., Guemouria, N., Chehbouni, A.H., Lahrouni, A., Olioso, A., Jacob, F., Williams, D.G., Sobrino, J.A., 2008. An integrated modelling and remote sensing approach for hydrological study in arid and semi-arid regions: The SUDMED programme. Int. J. Remote Sens. 29, 5161–5181. https://doi.org/10.1080/01431160802036417
Crow, W., Kustas, W., Prueger, J., 2008. Monitoring root-zone soil moisture through the assimilation of a thermal remote sensing-based soil moisture proxy into a water balance model. Remote Sens. Environ. 112, 1268–1281. https://doi.org/10.1016/j.rse.2006.11.033
Dejonge, K.C., Taghvaeian, S., Trout, T.J., Comas, L.H., 2015. Comparison of canopy temperature-based water stress indices for maize. Agric. Water Manag. 156, 51–62. https://doi.org/10.1016/j.agwat.2015.03.023
Diarra, A., Jarlan, L., Er-Raki, S., Le Page, M., Aouade, G., Tavernier, A., Boulet, G., Ezzahar, J., Merlin, O., Khabba, S., 2017. Performance of the two-source energy budget (TSEB) model for the monitoring of evapotranspiration over irrigated annual crops in North Africa. Agric. Water Manag. 193, 71–88. https://doi.org/10.1016/j.agwat.2017.08.007
Duchemin, B., Hadria, R., Erraki, S., Boulet, G., Maisongrande, P., Chehbouni, A., Escadafal, R., Ezzahar, J., Hoedjes, J.C.B., Kharrou, M.H., Khabba, S., Mougenot, B., Olioso, A., Rodriguez, J.-C., Simonneaux, V., 2006. Monitoring wheat phenology and irrigation in Central Morocco: On the use of relationships between evapotranspiration, crops coefficients, leaf area index and remotely-sensed vegetation indices. Agric. Water Manag. 79, 1–27. https://doi.org/10.1016/j.agwat.2005.02.013
Duchemin, B., Hagolle, O., Mougenot, B., Benhadj, I., Hadria, R., Simonneaux, V., Ezzahar, J., Hoedjes, J., Khabba, S., Kharrou, M.H., Boulet, G., Dedieu, G., Er-Raki, S., Escadafal, R., Olioso, A., Chehbouni, A.G., 2008. Agrometerological study of semi-ard areas: An experiment for analysing the potential of time series of FORMOSAT-2 images (Tensift-Marrakech plain). Int. J. Remote Sens. 29, 5291–5300. https://doi.org/10.1080/01431160802036482

Er-Raki, S., Chehbouni, A., Duchemin, B., 2010. Combining satellite remote sensing data with the FAO-56 dual approach for water use mapping in irrigated wheat fields of a semi-arid region. Remote Sens. 2, 375–387. https://doi.org/10.3390/rs2010375

Er-Raki, S., Chehbouni, A., Guemouria, N., Duchemin, B., Ezzahar, J., Hadria, R., 2007. Combining FAO-56 model and ground-based remote sensing to estimate water consumptions of wheat crops in a semi-arid region. Agric. Water Manag. 87, 41–54. https://doi.org/10.1016/j.agwat.2006.02.004

Er-Raki, S., Chehbouni, A., Hoedjes, J., Ezzahar, J., Duchemin, B., Jacob, F., 2008. Improvement of FAO-56 method for olive orchards through sequential assimilation of thermal infrared-based estimates of ET. Agric. Water Manag. 95, 309–321. https://doi.org/10.1016/j.agwat.2007.10.013

González-Dugo, M.P., Mateos, L., 2008. Spectral vegetation indices for benchmarking water productivity of irrigated cotton and sugarbeet crops. Agric. Water Manag. 95, 48–58. https://doi.org/10.1016/j.agwat.2007.09.001

Gutman, G., Ignatov, A., 1998. The derivation of the green vegetation fraction from NOAA / AVHRR. Int. J. Remote Sens. 19, 1533–1543.

Hain, C.R., Crow, W.T., Anderson, M.C., Mecikalski, J.R., 2012. An ensemble Kalman filter dual assimilation of thermal infrared and microwave satellite observations of soil moisture into the Noah land surface model. Water Resour. Res. 48. https://doi.org/10.1029/2011WR011268

Hain, C.R., Mecikalski, J.R., Anderson, M.C., 2009. Retrieval of an Available Water-Based Soil Moisture Proxy from Thermal Infrared Remote Sensing. Part I: Methodology and Validation. J. Hydrometeorol. 10, 665–683. https://doi.org/10.1175/2008JHM1024.1

Hunsaker, D.J., Pinter, P.J., Kimball, B.A., 2005. Wheat basal crop coefficients determined by normalized difference vegetation index. Irrig. Sci. 24, 1–14. https://doi.org/10.1007/s00271-005-0001-0

Ihuoma, S.O., Madramootoo, C.A., 2017. Recent advances in crop water stress detection. Comput. Electron. Agric. 141, 267–275. https://doi.org/10.1016/j.compag.2017.07.026

Jarlan, L., Khabba, S., Er-Raki, S., Le Page, M., Hanich, L., Fakir, Y., Merlin, O., Mangiarotti, S., Gascoin, S., Ezzahar, J., Kharrou, M.H., Berjamy, B., Saaïdi, A., Boudhar, A., Benkaddour, A., Laftouhi, N., Abaoui, J., Tavernier, A., Boulet, G., Simonneaux, V., Driouech, F., El Adnani, M., El Fazziki, A., Amenzou, N., Raibi, F., El Mandour, A., Ibouh, H., Le Dantec, V., Habets, F., Tramblay, Y., Mougenot, B., Leblanc, M., El Faïz, M., Drapeau, L., Coudert, B., Hagolle, O., Filali, N., Belaqziz, S., Marchane, A., Szczypta, C., Toumi, J., Diarra, A., Aouade, G., Hajhouji, Y., Nassah, H., Bigeard, G., Chirouze, J., Boukhari, K., Abourida, A., Richard, B., Fanise, P., Kasbani, M., Chakir, A., Zribi, M., Marah, H., Naimi, A., Mokssit, A., Kerr, Y., Escadafal, R., 2015. Remote Sensing of Water Resources in Semi-Arid Mediterranean Areas: the joint international laboratory TREMA. Int. J. Remote Sens. 36, 4879–4917. https://doi.org/10.1080/01431161.2015.1093198

Kalma, J.D., McVicar, T.R., McCabe, M.F., 2008. Estimating land surface evaporation: A review of methods using remotely sensed surface temperature data. Surv. Geophys. 29, 421–469. https://doi.org/10.1007/s10712-008-9037-z

Kite, G.W., Droogers, P., 2000. Comparing evapotranspiration estimates from satellites, hydrological models and field data. J. Hydrol. 229, 3–18. https://doi.org/10.1016/S0022-1694(99)00195-X

Kullberg, E.G., DeJonge, K.C., Chávez, J.L., 2016. Evaluation of thermal remote sensing

indices to estimate crop evapotranspiration coefficients. Agric. Water Manag. 179, 64–73. https://doi.org/10.1016/j.agwat.2016.07.007

Li, F., Crow, W.T., Kustas, W.P., 2010. Towards the estimation root-zone soil moisture via the simultaneous assimilation of thermal and microwave soil moisture retrievals. Adv. Water Resour. 33, 201–214. https://doi.org/10.1016/j.advwatres.2009.11.007

Li, Z.-L., Tang, R., Wan, Z., Bi, Y., Zhou, C., Tang, B., Yan, G., Zhang, X., 2009. A review of current methodologies for regional evapotranspiration estimation from remotely sensed data. Sensors (Basel). 9, 3801–53. https://doi.org/10.3390/s90503801

Long, D., Singh, V.P., 2012. A Two-source Trapezoid Model for Evapotranspiration (TTME) from satellite imagery. Remote Sens. Environ. 121, 370–388. https://doi.org/10.1016/j.rse.2012.02.015

Merlin, O., 2013. An original interpretation of the wet edge of the surface temperature-albedo space to estimate crop evapotranspiration (SEB-1S). Hydrol. Earth Syst. Sci. 17, 3623–3637. https://doi.org/10.5194/hess-17-3623-2013

Merlin, O., Chirouze, J., Olioso, A., Jarlan, L., Chehbouni, G., Boulet, G., 2014. An image-based four-source surface energy balance model to estimate crop evapotranspiration from solar reflectance/thermal emission data (SEB-4S). Agric. For. Meteorol. 184, 188–203. https://doi.org/10.1016/j.agrformet.2013.10.002

Merlin, O., Rüdiger, C., Bitar, A. Al, Richaume, P., Walker, J.P., Kerr, Y.H., 2012. Disaggregation of SMOS Soil Moisture in Southeastern Australia. IEEE Trans. Geosci. Remote Sens. 50, 1556–1571.

Moran, M.S., Clarke, T.R., Inoue, Y., Vidal, A., 1994. Estimating Crop Water Deficit Using the Relation between Surface-Air Temperature and Spectral Vegetation Index. Remote Sens. Environ. 49, 246–263.

Olioso, A., Sòria, G., Sobrino, J., Duchemin, B., 2007. Evidence of Low Land Surface Thermal Infrared Emissivity in the Presence of Dry Vegetation. IEEE Geosci. Remote Sens. Lett. 4, 112–116.

Olivera-Guerra, L., Mattar, C., Merlin, O., Durán-Alarcón, C., Santamaría-Artigas, A., Fuster, R., 2017. An operational method for the disaggregation of land surface temperature to estimate actual evapotranspiration in the arid region of Chile. ISPRS J. Photogramm. Remote Sens. 128, 170–181. https://doi.org/10.1016/j.isprsjprs.2017.03.014

Rafi, Z., Merlin, O., Le Dantec, V., Khabba, S., Mordelet, P., Er-Raki, S., Amazirh, A., Olivera-Guerra, L., Aït Hssaine, B., Simonneaux, V., Ezzahar, J., Ferrer F. 2018. Partitioning evapotranspiration of drip-irrigated wheat crop: a comparison study of FAO-56 dual crop coefficient model estimates with eddy covariance, sap flow and lysimeter measurements. Agric. For. Meteorol. *Under review*.

Roerink, G.J., Su, Z., Menenti, M., 2000. S-SEBI: A simple remote sensing algorithm to estimate the surface energy balance. Phys. Chem. Earth, Part B Hydrol. Ocean. Atmos. 25, 147–157. https://doi.org/10.1016/S1464-1909(99)00128-8

Sandholt, I., Rasmussen, K., Andersen, J., 2002. A simple interpretation of the surface temperature/vegetation index space for assessment of surface moisture status. Remote Sens. Environ. 79, 213–224. https://doi.org/10.1016/S0034-4257(01)00274-7

Sobrino, J.A., Jiménez-muñoz, J.C., Sòria, G., Romaguera, M., Guanter, L., Moreno, J., Plaza, A., Martínez, P., 2008. Land Surface Emissivity Retrieval From Different VNIR and TIR Sensors. IEEE Trans. Geosci. Remote Sens. 46, 316–327.

Toumi, J., Er-Raki, S., Ezzahar, J., Khabba, S., Jarlan, L., Chehbouni, A., 2016. Performance assessment of AquaCrop model for estimating evapotranspiration, soil water content

and grain yield of winter wheat in Tensift Al Haouz (Morocco): Application to irrigation management. Agric. Water Manag. 163, 219–235. https://doi.org/10.1016/j.agwat.2015.09.007
Weng, Q., Fu, P., Gao, F., 2014. Generating daily land surface temperature at Landsat resolution by fusing Landsat and MODIS data. Remote Sens. Environ. 145, 55–67. https://doi.org/10.1016/j.rse.2014.02.003

Tables

Table 1. Sowing and irrigation dates.

Sowing and irrigation event	Date	Days after sowing (DAS)
Sowing date	14 January	0
First irrigation	4 February	22
Second irrigation	20 March	66
Third irrigation	13 April	90
Fourth irrigation	21 April	98

Figures

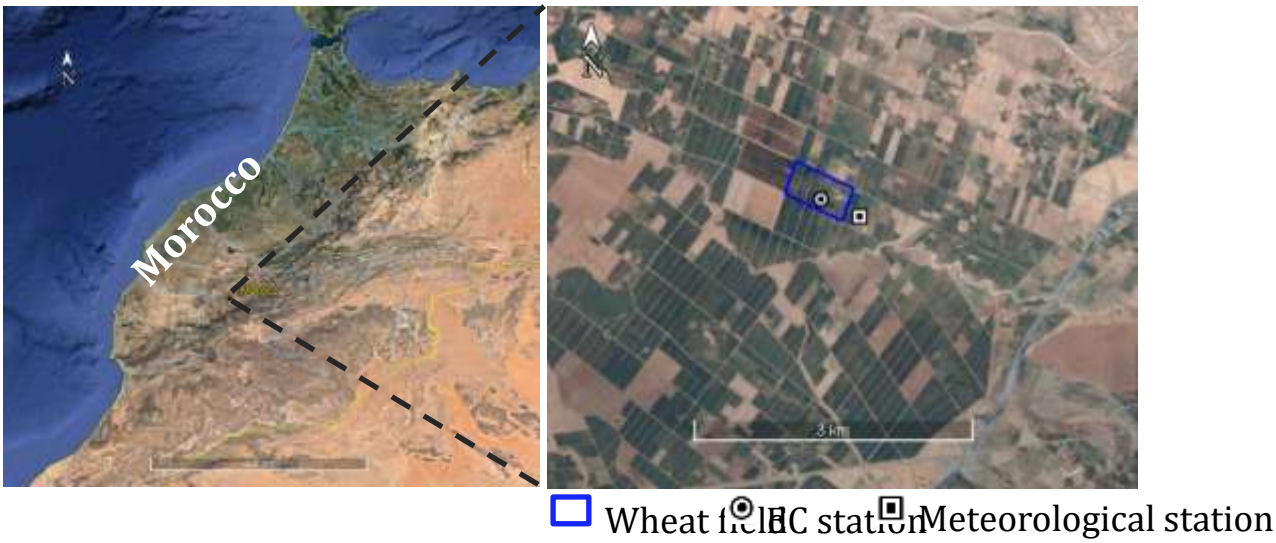

Fig. 1. Study area.

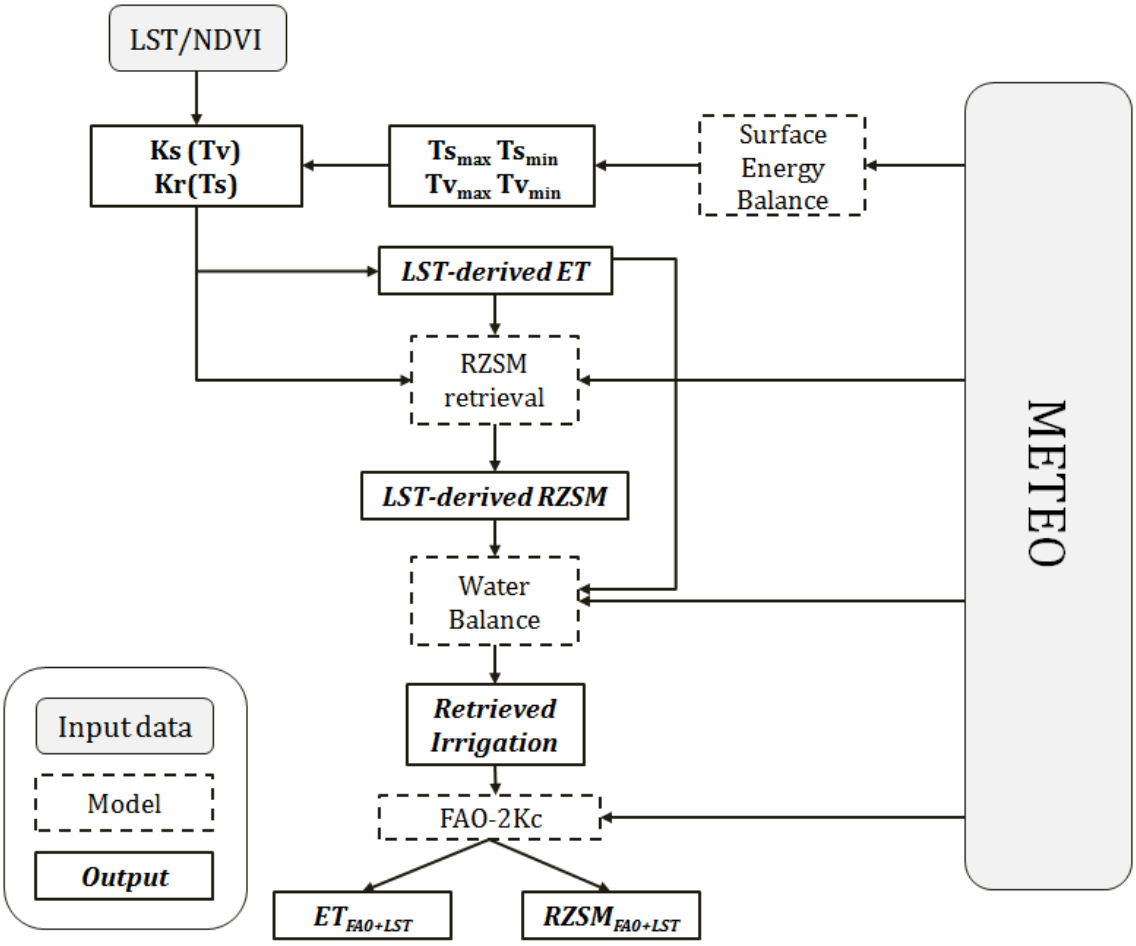

Fig.2. Schematic diagram presenting an overview of the main inputs, models and outputs of the LST-integrated FAO-2Kc approach.

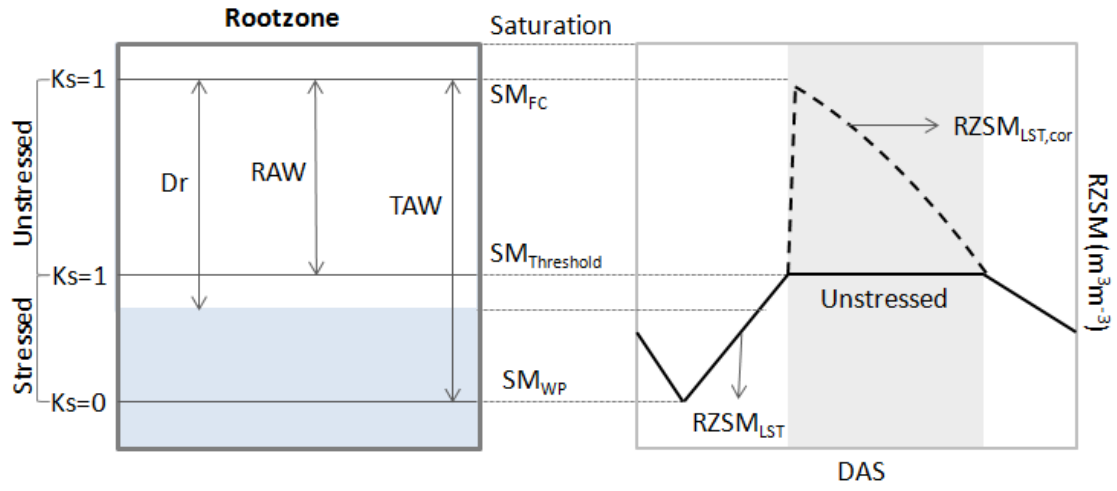

Fig. 3. Schematic representation of RZSM retrieval for stressed (Ks < 1) and unstressed (Ks = 1) periods. The left box represents the variation of RZSM according to the depletion (Dr) in the rootzone. Following the FAO-2Kc formulations, RZSM ranges between SM_{WP} and SM_{FC}, which constrain the total available water (TAW) and readily available water (RAW = p TAW). The right plot represents the temporal variability of LST-derived RZSM, where is showed an unstressed period (shaded area) for which $RZSM_{LST}$ (equal to $SM_{threshold}$) is corrected for both LST-derived ET and precipitation through a daily water budget.

a)

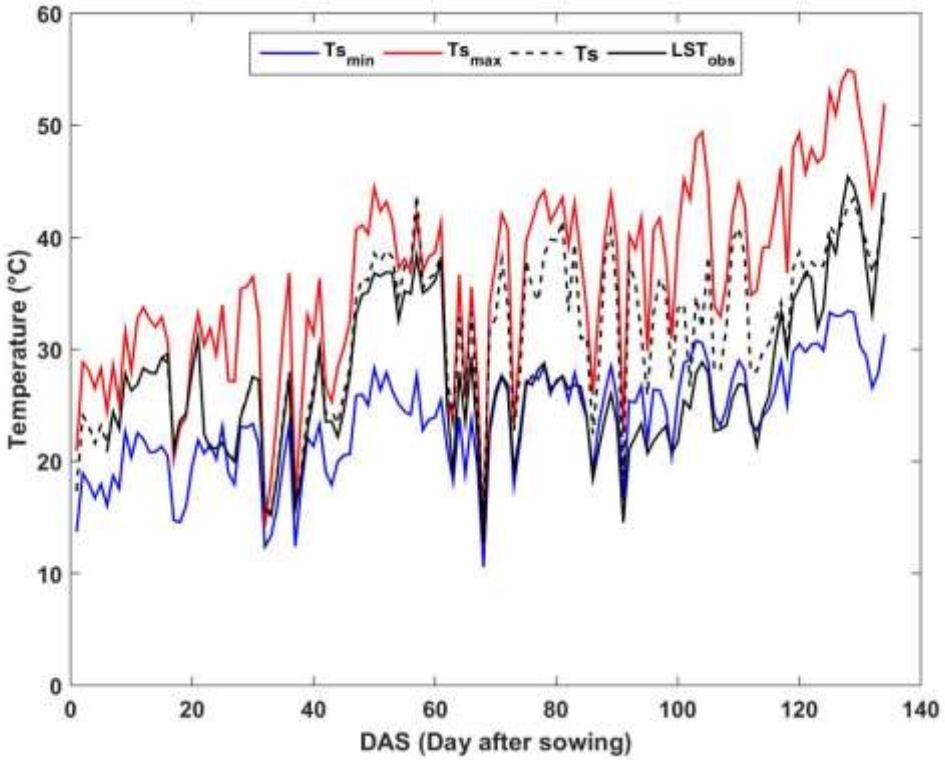

b)

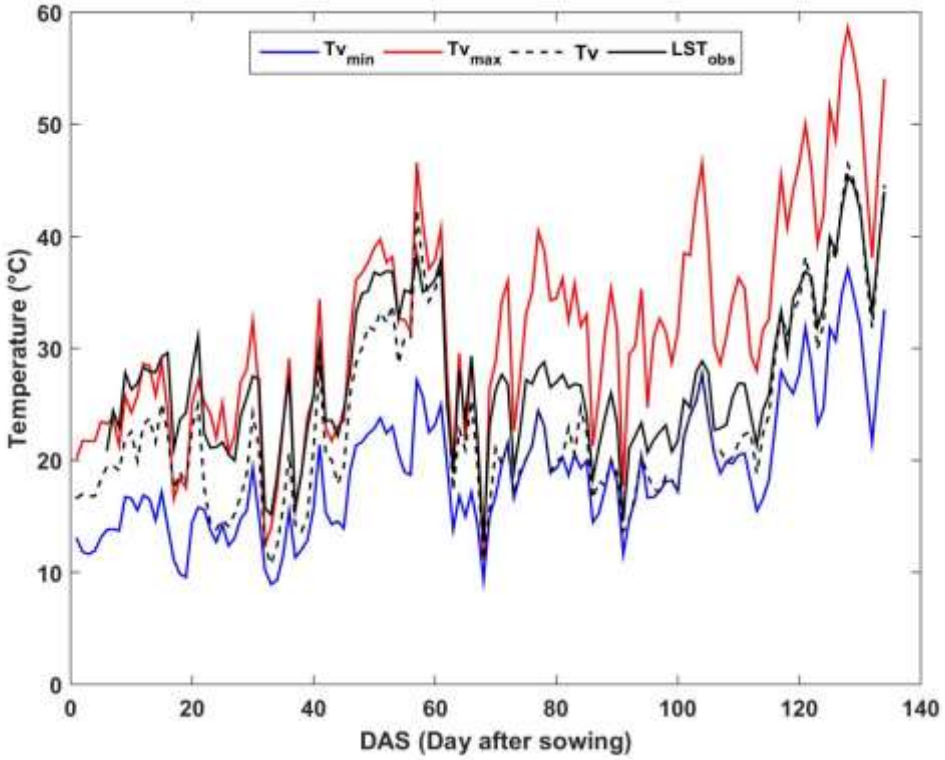

Fig. 4. Time series of (a) Ts_{min}, Ts_{max} and Ts estimates and (b) Tv_{min}, Tv_{max} and Tv estimates. Ground-based LST (LST_{obs}) is also shown on both plots for comparison.

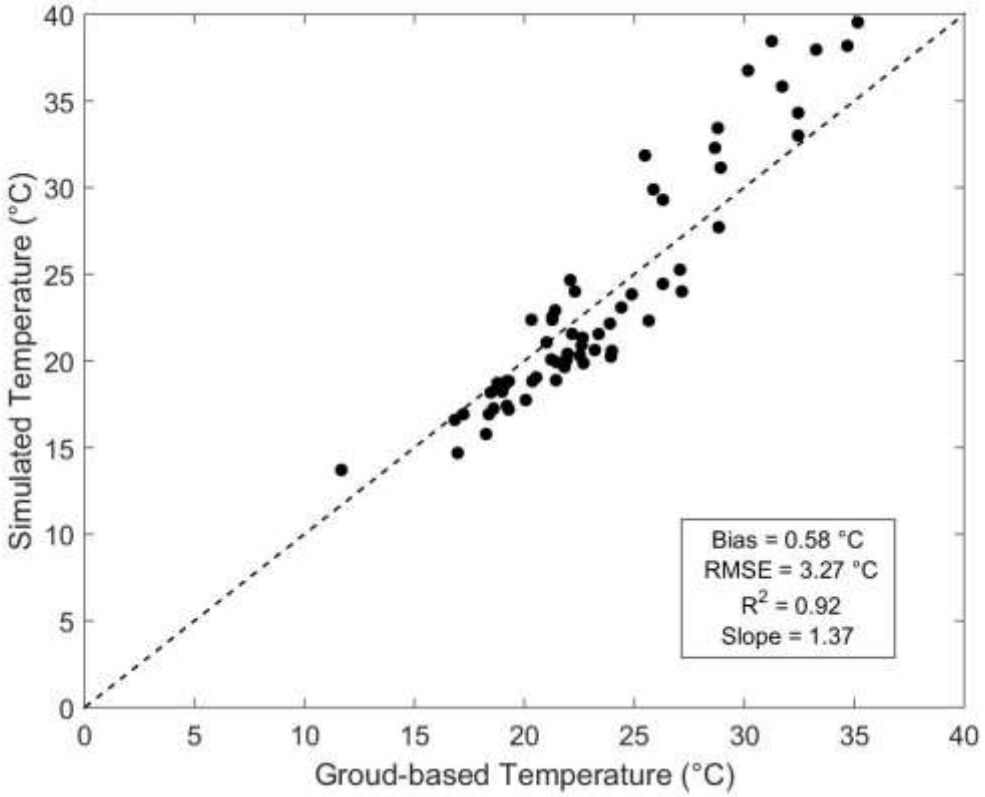

Fig. 5. Retrieved versus ground-based vegetation temperature (average of the 7 thermocouples between 10 am and 2 pm) for the period with fc>0.5 (between DAS 69 and 134).

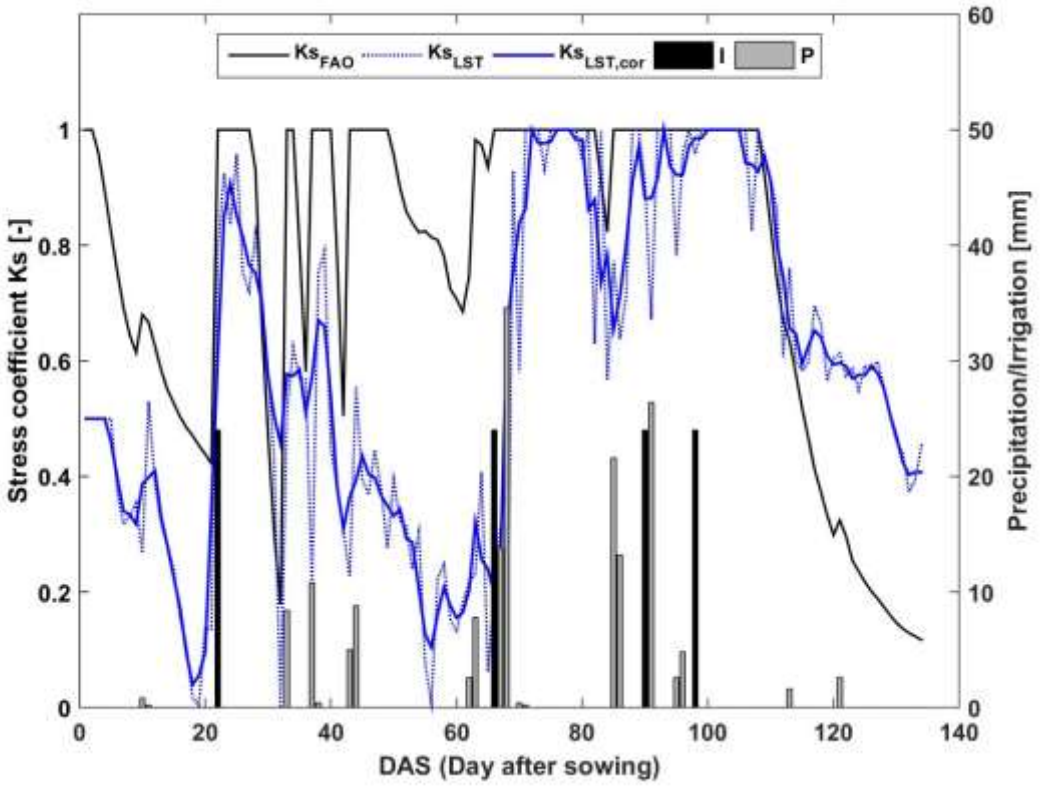

Fig 6. Ks from FAO-2Kc method according to Allen et al. 1998 (Ks_{FAO}), LST-derived Ks from daily ground-based LST (Ks_{LST}) and the smoothed LST-derived Ks ($Ks_{LST,cor}$). Precipitation (P) and irrigation (I) amounts are also shown.

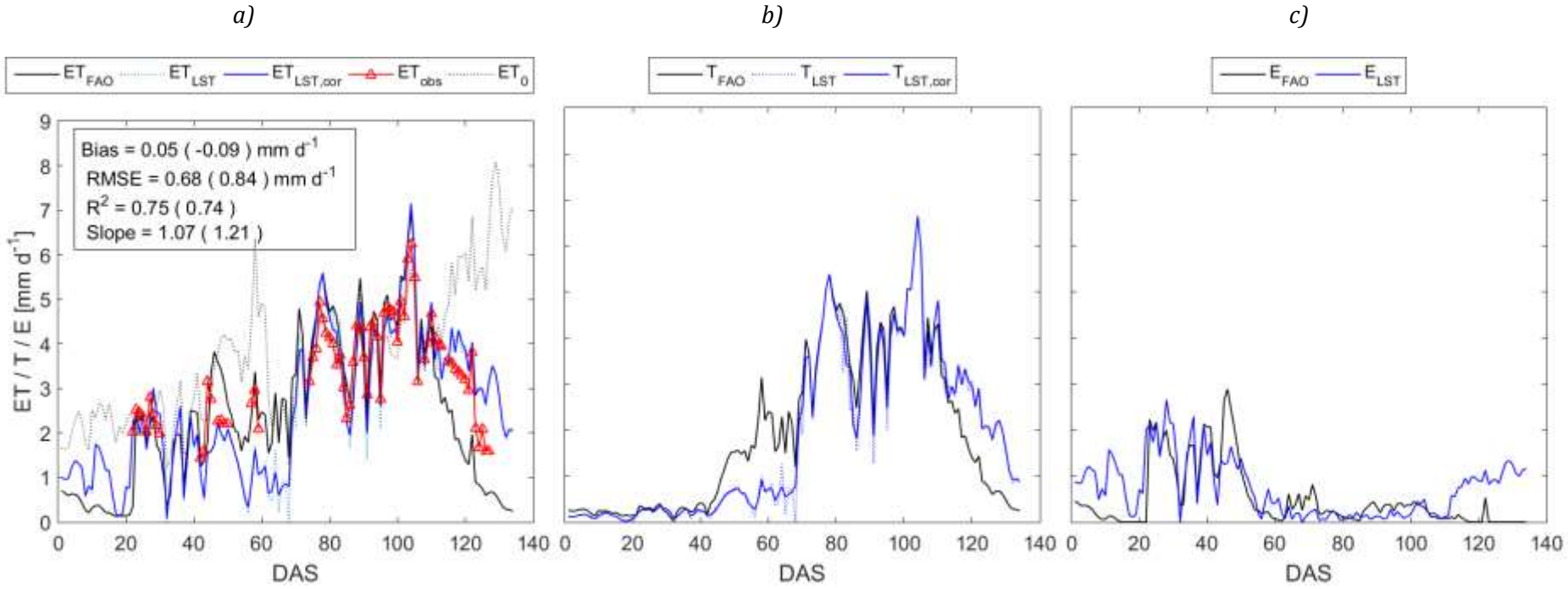

Fig. 7. Time series of daily (a) ET, (b) T and (c) E estimates from FAO-2Kc method using the parameters given by Allen et al (1998) forced by observed irrigation, and from LST-derived Ks (ET and T) and LST-derived Kr (E) and from the smoothed LST-derived Ks (ET_{cor} and T_{cor}, respectively). The statistical parameters of ET_{cor} (ET_{FAO}) versus EC observations are shown in the box of (a).

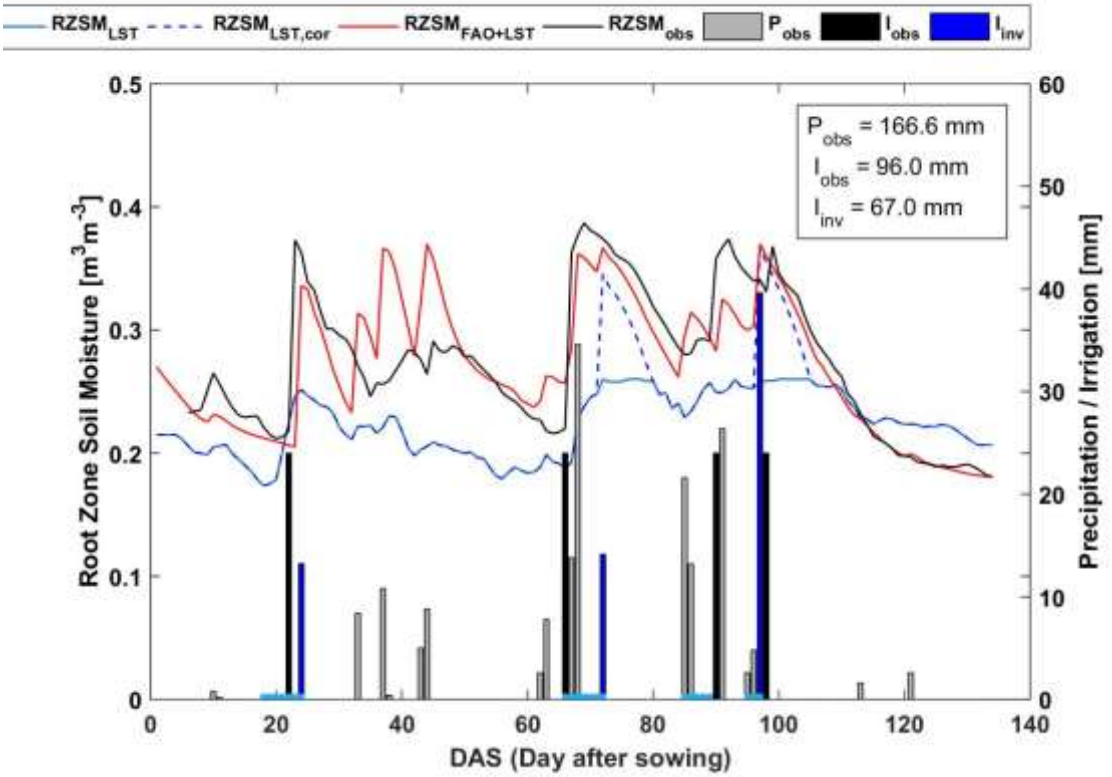

Fig. 8. Time series of LST-derived RZSM for stressed periods when Ks<1 ($RZSM_{LST}$), corrected LST-derived RZSM ($RZSM_{LST,cor}$) through a water budget for unstressed periods when Ks=1 and the RZSM simulated by the FAO-2Kc ($RZSM_{FAO+LST}$) by using precipitation (P_{obs}) and retrieved irrigation (I_{inv}) as input. The periods of significant increase in $RZSM_{LST,cor}$ are marked in the x axis (cyan). Observed precipitation, irrigation and RZSM are also shown for comparison. The observed cumulated precipitation (P_{obs}), irrigation (I_{obs}) and retrieved irrigation (I_{inv}) are shown.

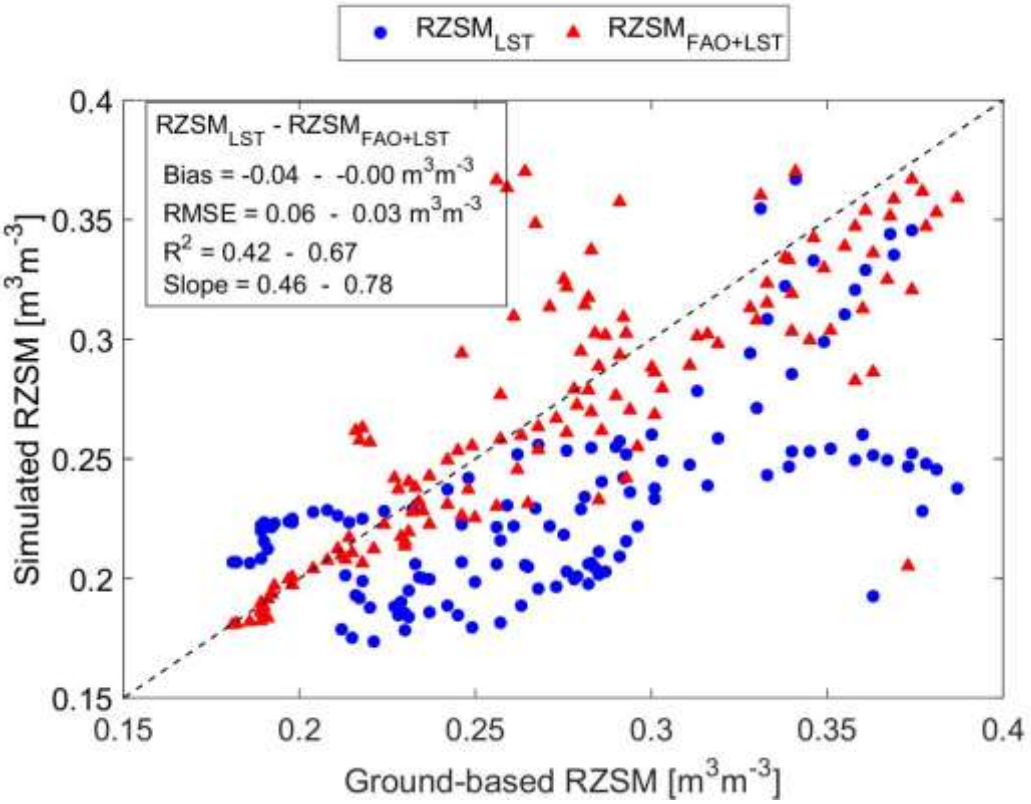

Fig. 9. LST-derived RZSM ($RZSM_{LST}$) and FAO-simulated RZSM by forcing the FAO-2Kc model using retrieved irrigation ($RZSM_{FAO+LST}$) versus ground-based RZSM.

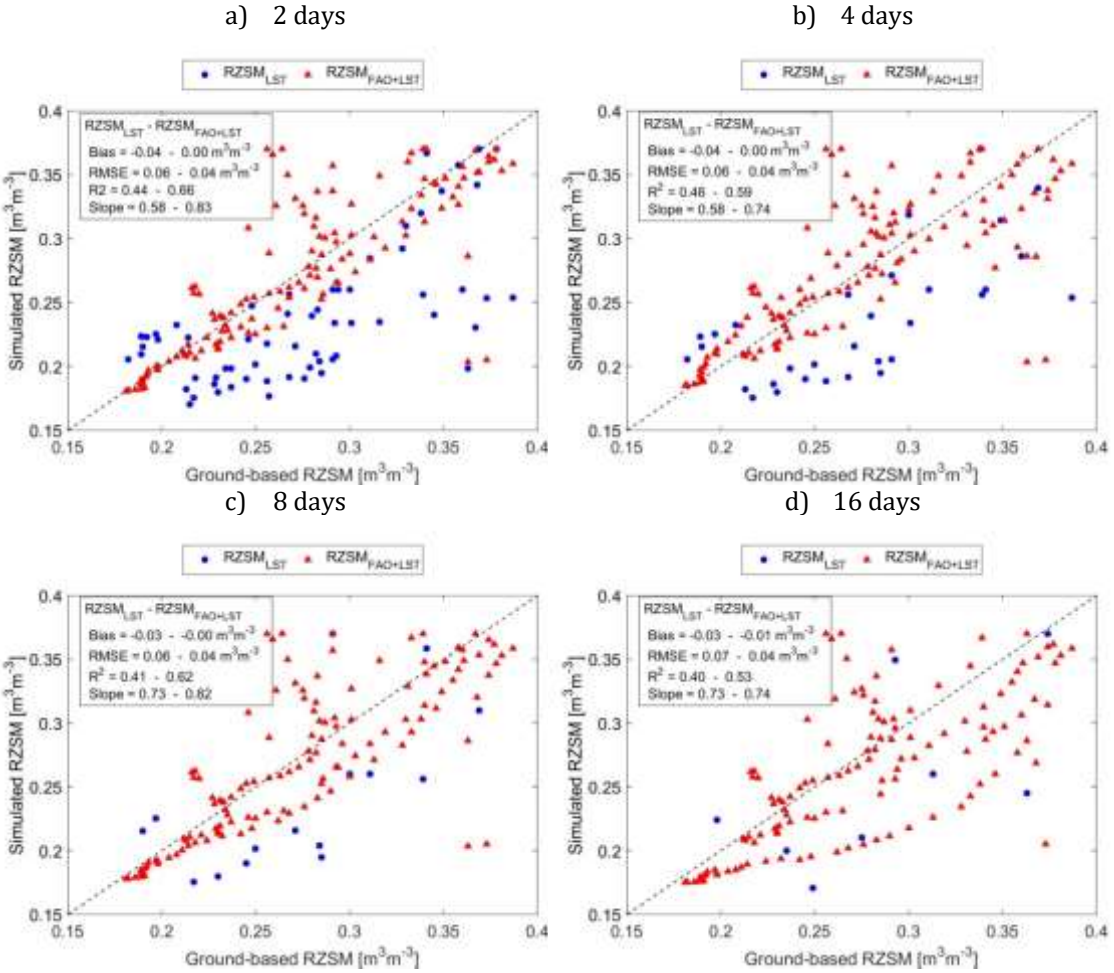

Fig. 10. Validation of the RZSM simulated by FAO-2Kc approach ($RZSM_{FAO+LST}$) by using observed precipitation and the irrigation retrieved from thermal observations available at a decreasing frequency (1 every 2, 4, 8 and 16 days). The statistical parameters of the LST-derived RZSM ($RZSM_{LST}$) are shown as a reference of the improvement of in $RZSM_{FAO+LST}$.

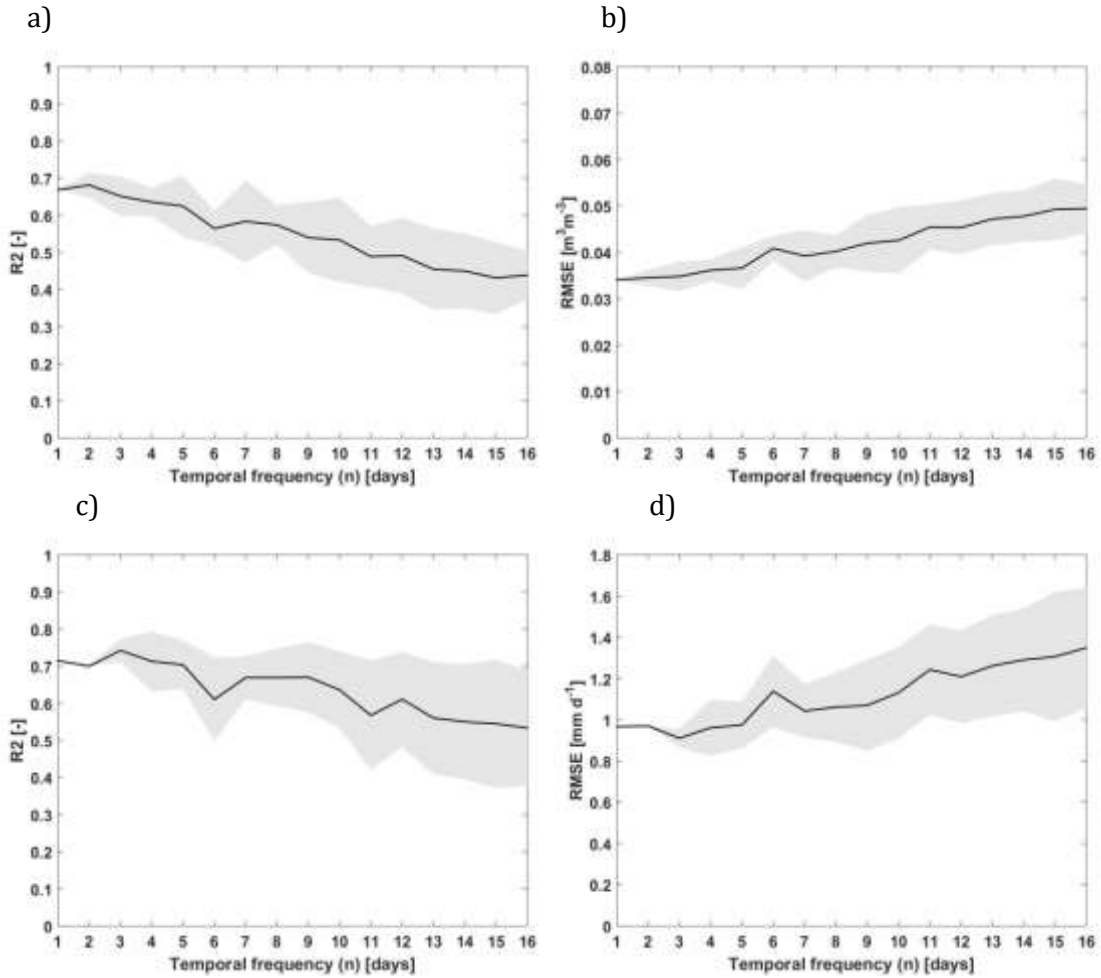

Fig. 11. Sensitivity of (a,b) $RZSM_{FAO+LST}$ and (c,d) re-analyzed ET (ET simulated from FAO-2Kc approach by using the input of precipitation and retrieved irrigation) to different frequency of thermal data observations. Average R^2 (a,c) and RMSE (b,d) are presented for each temporal frequency by running the model n times by changing the first day of observation from 1 to n. The shaded area represents its standard deviation.

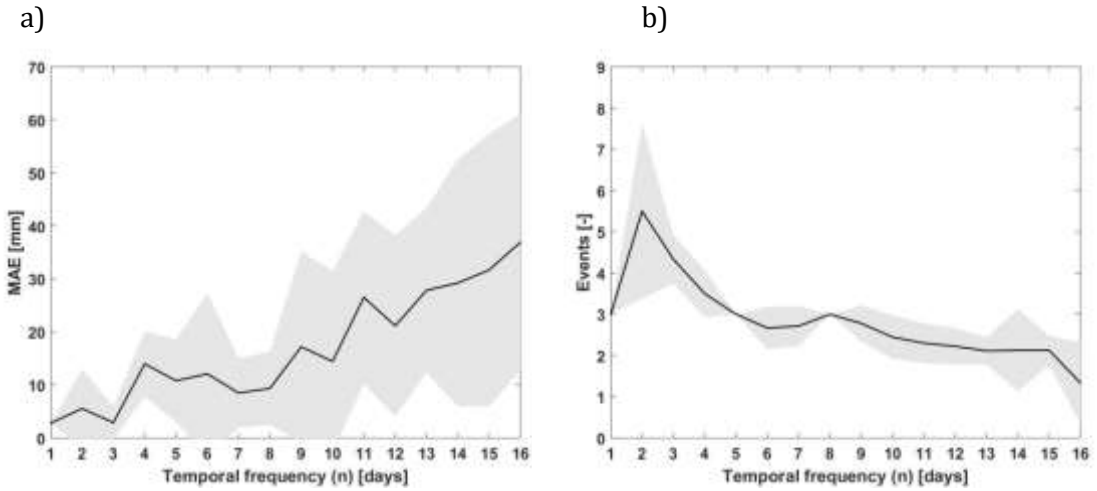

Fig. 12. Sensitivity of total irrigation water supply constrained from LST-derived ET and RZSM to different frequency of thermal data observations. (a) Average mean absolute error (MAE) of total irrigation water supply and (b) number of retrieved irrigation events are presented for each temporal frequency where the model is run n times by changing the start day from 1 to n. The shaded area represents its standard deviation. The observed total irrigation water supply is equal to 96 mm (69.8 mm without drainage) distributed in 4 events during the wheat growing season.